A Multiaxial Fatigue Damage Model for Fibre Reinforced Polymer Composites

A MULTIAXIAL FATIGUE DAMAGE MODEL FOR FIBRE REINFORCED POLYMER COMPOSITES

C. R. Kennedy[1], C. M. Ó Brádaigh, S. B. Leen

Mechanical Engineering, NUI Galway, Ireland

Abstract: A multiaxial fatigue damage model for fibre reinforced polymer composite materials is presented. The model combines (i) fatigue-induced fibre strength and modulus degradation, (ii) irrecoverable cyclic strain effects and (iii) inter-fibre fatigue. The inter-fibre fatigue aspect is based on a fatigue-modified version of the Puck multiaxial failure criterion for static failure. The model is implemented in a user material finite element subroutine and calibrated against fatigue test data for unidirectional glass fibre epoxy. A programme of uniaxial fatigue tests on quasi-isotropic glass fibre epoxy laminates is presented for validation of the novel fatigue damage methodology. The latter is successfully validated across a range of stress levels.

1 Introduction

Glass-fibre reinforced polymers (GFRP) are candidate low cost materials for use in ocean energy structures. Quasi-isotropic (QI) laminates are useful where (i) the loads are not very well understood, or (ii) the loads are complex and multi-directional in nature, both of which are relevant to the ocean energy (e.g. tidal turbine) application, which is a novel application. It is anticipated that long-term durability of materials will be a key factor in the success of candidate ocean energy devices. Hence, the fatigue of QI laminates is investigated as here part of a larger research programme investigating the fatigue behaviour of GFRP laminates while immersed in seawater.

Micromechanical approaches to fatigue modelling are preferred because they offer the possibility of being able to model any laminate configuration with any combination of applied loads. A convenient level for modelling is the single unidirectional (UD) ply level as these models can then be combined in a computer simulation of any laminate configuration.

Talreja described the fatigue damage mechanisms in a UD ply based on strain levels and subsequently when it is embedded in a laminate [1]. It was found that matrix and interfacial cracking occurred first parallel to the fibres, in the most off-axis ply, caused by a combination of transverse normal and shear loading on the ply. In epoxy/E-glass cracking started with localised transverse fibre debonding at approximately 0.12% strain in 90° plies and became full width (of test coupon) and of ply thickness by 0.42% strain [2] (termed inter fibre fracture (IFF) [3]). Fatigue cycling of an epoxy/E-glass laminate between 0 and 0.33% strain was found to initiate IFF in the 90° ply at the coupon edges around 3,500 cycles and these fractures propagated in both length and density at a steady rate [4]. Higher peak (cyclic) strains were found to increase the rate and maximum density of IFF in 90° plies.

Analysis of IFF initiation strain in plies at angles other than 90° is facilitated using composite laminate theory (CLT) to calculate the strains in the ply orientation. For example, Talreja

[1] Corresponding author. Tel.: +353 91493020; Fax.: +353 91563991; E-mail address: c.kennedy8@nuigalway.ie

presents evidence that IFF crack initiation in 45° angle ply epoxy/E-glass laminates occurs at 0.4% peak fatigue strain in the global 0° direction. Using CLT this corresponds to an in-plane shear strain (γ_{12}) of 0.65% and normal strains (ε_1 and ε_2) of 0.07%. Others have tested epoxy/E-glass laminate tubes with a torsional loading which places one of the laminate plies under pure shear stress [5]. Evidence of IFF initiation is seen in this ply when the shear stress reaches 0.8%. The Tsai-Hill criterion is a reasonable approximation for data from these kinds of experiments when various ratios of γ_{12} and ε_2 are tested [6]. However in a recent comparison of many static failure theories against experimental data, the Tsai-Hill criterion was shown to be significantly non-conservative in predicting IFF in biaxial compression, whereas the Puck criterion was shown to be a good predictor of IFF under any loading condition [7].

The second damage mechanism relevant to fatigue of laminates is delamination at the interface between plies [8]. This occurs at free edges, holes or where through-the-thickness tensile stresses are present [9]. Local delamination also occurs at the intersection of cracks at interfaces in QI laminates under uniaxial fatigue [2]. This type of failure is more important in laminates without fibres closely aligned to the principal load [10].

The third damage mechanism is fatigue damage in the fibre direction. As tensile strain levels approach the matrix material fatigue limit; voids, early fibre breaks, cracks in adjacent plies or other imperfections initiate matrix cracks perpendicular to the fibre (e.g. 0.6% strain in epoxy/E-glass [11]). These cracks then act as stress concentrations for nearby fibres and cause additional fibre fracture. This damage progresses under fatigue cycling and groups of fibre breaks form at each of the initiation sites. Growth of these damaged areas is usually slow and most of the fatigue life is taken up while these areas slowly grow in size. Longitudinal cracks also form and facilitate coalescence of these fibre breaks regions. Finally a network of connected cracks form through the ply cross section which leads to failure of the on-axis ply and quickly leads to complete fracture of the laminate. The effects of this are stiffness reduction, irrecoverable strain and strength reduction.

A review of fatigue models in 2001 documented approximately 60 different fatigue models [12]. Many of the models were focused on particular laminates or laminate types but as computational power has increased, ply-by-ply approaches have become increasingly popular as they can be applied to any laminate. The stress exposure approach has been used both in static [13] and fatigue models [14] [15] using bespoke software code. This paper presents a finite element implementation of a new fatigue damage model for a QI laminate undergoing fatigue cycling. A user defined material subroutine is developed using a combination of the Puck stress exposure technique and fibre direction degradation. This subroutine is implemented in a unit cell finite element model of the laminate to predict the fatigue degradation response. The results of the model are compared to experimental results measuring modulus degradation, irrecoverable strain and fatigue life.

2 Experimental Method

Quasi-isotropic laminates have been manufactured using the VARTM (Vacuum Assisted Resin Transfer Moulding) process. Non-woven stitched glass-fibre material with 300 g/m^2 per ply is stacked to create a $[(45\backslash 135\backslash 90\backslash 0)_2]_s$ laminate. Epoxy resin is introduced under vacuum to complete the laminate. After a room temperature cure for 48 hours, the laminates are oven cured at 80° C for approximately 4 hours. Fibre volume fractions (V_f) of 50% were achieved at an average thickness of 3.75 mm. The laminates are cut into 25 x 250 mm coupons using a water cooled diamond abrasive disk.

Fatigue tests are performed with an Instron 8801 test machine and 8800 digital controller applying a constant amplitude sinusoidal force in tension-tension mode (R = 0.1) between 3 and 6 Hz. The frequency is decreased as the stress level increases to avoid internal heating of the test coupon and a fan is used to cool the coupons during testing. Infra-red thermometer measurements on similar tests had shown success in keeping coupon temperature rise at less than 10° C during fatigue cycling. Twenty coupons were tested over a range of maximum stress levels that caused the coupons to fail between 3000 cycles and 1 million cycles. The number of cycles to failure and stress applied to each coupon is recorded thereby producing a stress-life (SN) curve.

During fatigue cycling the load and displacement are monitored continuously and the maxima and minima of both are recorded at every 10th cycle. This allows the drop in tensile modulus and increase in irrecoverable strain of the coupon during fatigue cycling to be obtained. Similar results were obtained by using an extensometer to measure strain over three slow cycles initially at the start of the fatigue test; the extensometer was then removed and the fatigue test continued for 5,000 cycles. At this point the coupon was removed and its overall length measured and compared to its original length to find the irrecoverable strain. The coupon was then reinstalled with the extensometer attached and 3 more slow cycles repeated to obtain the modulus of the material at that point in the fatigue life. This procedure was repeated throughout the fatigue life of the three coupons tested using this technique.

3 Modelling

In this paper modelling of the GFRP laminates is implemented via a finite element (FE) methodology as shown in Figure 1. The FE code uses elastic analysis to calculate the strains at each point in the laminate and to translate those strains into the local material coordinates. The user material subroutine developed here then computes the (non-linear) behaviour of each material point depending on its stress history and number of fatigue cycles accumulated. The subroutine calculates; firstly the fibre direction response to on-axis (1-direction) tensile/compressive stresses, and secondly the matrix response to transverse normal (2 and 3-direction) stresses and/or shear stresses. The FE code then integrates the response of all the elements (gauss points) and checks for global equilibrium and convergence.

3.1 Fibre direction model

Three fibre direction fatigue effects that are modelled in this work; strength degradation, modulus degradation and irrecoverable strain (creep). 0° testing of unidirectional laminates under tensile or compressive loads provides data on the effects of fatigue on the material in the fibre direction. Experimentally derived stress-life (SN) or strain-life (ε-N) curves [16] are also employed.

3.1.1 Fibre direction strength degradation

The degradation of fibre direction strength during fatigue cycling is assumed to follow a simple linear degradation per cycle. This has the advantage that only the expected life at each stress level is needed and this can be obtained from the SN curve or constant life diagram. A comparison of many candidate models recently concluded that the linear model was preferred based on its simplicity and conservative predictions [17]. The residual strength in the fibre direction is given by [18]

$$R_{\parallel}^{r} = R_{\parallel}^{s} - \sum_{i=1}^{m} (R_{\parallel}^{s} - \sigma_{max}^{i}) \frac{\Delta n_i}{N_f(\sigma_{max}^{i})} \tag{1}$$

where m is the number of fatigue cycle blocks, Δn_i is the number of fatigue cycles in block i $R_{\parallel}^{r}$ is the residual strength after the i blocks, $R_{\parallel}^{s}$ is the static fibre direction strength, σ_{max}^{i} is the maximum stress during the i^{th} block and N_f is the number of cycles to failure in constant amplitude fatigue at σ_{max}^{i}. N_f is obtained from the SN curve of UD material which is often approximated with a power function of the form

$$\sigma_{max} = AN_f^{-B} \tag{2}$$

Figure 2 shows a schematic of the drop in fibre direction strength due to a complex load history. This schematic is based on the properties of UD 50% V_f GFRP and is composed of blocks of different stress levels each with different mean and alternating stress levels. Fracture occurs when residual strength degrades to a level at or below the stress levels developed during any fatigue cycle.

3.1.2 Fibre direction fatigue modulus degradation

Experimental testing has shown that early stage damage occurs during initial fatigue cycling in the fibre direction followed by a long period where the damage accumulation rate is quite low. Finally the accumulated damage reduces the capacity of the material to resist the stresses and there is a relatively rapid drop to failure. The modulus of the material is reduced as damage increases. True modulus is difficult to measure experimentally in fatigue testing and therefore secant modulus and fatigue modulus are used here instead. Fatigue modulus is defined here as the slope of a line which connects the minimum stress-strain point in a fatigue cycle with the maximum stress-strain point in the cycle as shown in Figure 3. Mao and Mahadevan [19] have proposed the following equation to represent the s-shaped damage evolution with number of cycles

$$D = q\left(\frac{n}{N_f}\right)^{m1} + (1-q)\left(\frac{n}{N_f}\right)^{m2} \tag{3}$$

where D is the accumulated damage at n number of cycles, N_f is the fatigue life (number of cycles) at the load being applied and q, $m1$, $m2$ are material dependent parameters. Figure 4 shows a schematic of the accumulation of damage during fatigue cycling.
The Mao and Mahadevan damage evolution equation is used here to predict the degradation in fibre direction fatigue modulus during fatigue as follows

$$E_{1d} = E_{1o} - \Delta E_1 D \tag{4}$$

where E_{1d} is the degraded fatigue modulus, E_{1o} is the original fatigue modulus and ΔE_1 is the drop in modulus between the first cycle and the cycle just prior to failure. The magnitude of ΔE_1 depends on the maximum fatigue stress $(\sigma_{1,max})$.

3.1.3 Irrecoverable strain in the fibre direction

Figure 3 shows the accumulation of irrecoverable strain under fatigue loading with a tensile maximum load. This is incorporated into the present fatigue damage model. The equation adopted here is based on the assumption that the irrecoverable strain (ε_{1cr}) increases in proportion to the change in fatigue modulus. The irrecoverable strain accompanying the modulus with damage D is:

$$\varepsilon_{1cr} = \frac{\varepsilon_{1f}(E_{1o} - E_{1d})}{(E_{1o} - E_{1f})} \tag{5}$$

where E_{1f} is the fatigue modulus at the start of the final cycle and ε_{1f} is the creep strain at the start of the final cycle.

3.2 Matrix governed response of UD lamina

Stresses in the lamina coordinate system (1,2,3) are translated into the fracture plane coordinate system (1,n,t) using vector transformation in the 2-3 plane as shown in Figure 5.
The key event in the transverse direction is IFF cracking of the lamina caused by a combination of transverse normal stress (σ_n) and shear stresses (τ_{n1}, τ_{nt}). Puck [20] has developed equations to predict IFF failure based on lamina strengths. These equations are modified here for fatigue degradation using the fatigue strengths of the lamina as follows:

$$f_E(\theta) = \sqrt{\left(\frac{\tau_{nt}}{R^A_{\perp\perp}(N)}\right)^2 + \left(\frac{\tau_{nl}}{R_{\perp\parallel}(N)}\right)^2 + \sigma_n^2\left(\frac{1}{R^{(+)}_{\perp}(N)} - \frac{p^{(+)}_{\perp\psi}}{R^A_{\perp\psi}(N)}\right)^2} + \frac{p^{(+)}_{\perp\psi}}{R^A_{\perp\psi}(N)}\sigma_n \tag{6}$$

$$\text{for } \sigma_n \geq 0$$

$$f_E(\theta) = \sqrt{\left(\frac{\tau_{nt}}{R^A_{\perp\perp}(N)}\right)^2 + \left(\frac{\tau_{nl}}{R_{\perp\parallel}(N)}\right)^2 + \sigma_n^2\left(\frac{p^{(-)}_{\perp\psi}}{R^A_{\perp\psi}(N)}\right)^2} + \frac{p^{(-)}_{\perp\psi}}{R^A_{\perp\psi}(N)}\sigma_n \tag{7}$$

for $\sigma_n < 0$

$$\frac{p^{(\pm)}_{\perp\psi}}{R^A_{\perp\psi}(N)} = \frac{1}{\tau_{nt}^2 + \tau_{nl}^2}\left(\frac{p^{(\pm)}_{\perp\perp}}{R^A_{\perp\perp}(N)}\tau_{nt}^2 + \frac{p^{(\pm)}_{\perp\parallel}}{R_{\perp\parallel}(N)}\tau_{nl}^2\right) \tag{8}$$

when $\tau_{nt}^2 + \tau_{nl}^2 > 0$, $\quad otherwise = 0$

$$R^A_{\perp\perp}(N) = \frac{R^{(-)}_{\perp}(N)}{2\left(1 + p^{(-)}_{\perp\perp}\right)} \tag{9}$$

$f_E(\theta)$, called the stress exposure, is a measure of the fraction along the path to IFF failure. At stresses below IFF, $f_E(\theta)$ is less than 1.0; failure is predicted when $f_E(\theta) = 1$. $R^A_{\perp\perp}(N)$ is the fatigue resistance to τ_{nt} (fibre rolling) shear stress, $R_{\perp\parallel}(N)$ is the fatigue resistance to τ_{nl} (fibre sliding) shear stress, $R^{(+)}_{\perp}(N)$ is the transverse tensile fatigue strength, $R^{(-)}_{\perp}(N)$ is the transverse compressive fatigue strength, $p^{(+)}_{\perp\perp}$, $p^{(-)}_{\perp\perp}$, $p^{(+)}_{\perp\parallel}$, $p^{(-)}_{\perp\parallel}$ are parameters which control the inclination of the failure envelope around zero transverse stress and have recommended values between 0.20 and 0.30 [20]. The transverse and shear fatigue strengths ($R^{(+)}_{\perp}(N)$, $R^{(-)}_{\perp}(N)$, $R_{\perp\parallel}(N)$) are all degraded using a function of the form

$$R(N) = R_o\left(1 - \sum_{i=1}^{m}\frac{\Delta n_i}{N_f(\sigma^i_{max})}\right) \tag{10}$$

where R_o is the original strength in question, R_i is the strength at cycle *i* and $N_f(\sigma^i_{max})$ is again given by the SN curve of the UD material for the strength in question with the form given in Equation 2.

3.2.1 Transverse and shear strength degradation under fatigue

Tong [2] presented data on number of fatigue cycles to IFF initiation in individual plies of an epoxy/E-glass QI laminate under uniaxial fatigue loading at various levels. First cycle stress exposure levels have been calculated for the plies in those laminates. This analysis used CLT to calculate the transverse and shear stresses in each ply, material strength values / inclination parameters for similar lamina [20] and the original versions of Equations 6 to 9 to calculate stress exposure. Figure 6 shows the results of this analysis; calculated stress exposure level at the start of the fatigue test are plotted against the number of cycles at which IFF was observed to occur. These data show the resistance to IFF decreases by 40% in 125,000 cycles.

Material strength values are important inputs to the stress exposure calculation and SN curves of transverse direction tensile fatigue cycling [16] show that transverse tensile strength degrades by approximately 50% in 100,000 cycles. Therefore for the model developed here it is assumed that degrading the transverse and shear strengths using Miner's rule and the fatigue SN curve is appropriate when calculating stress exposure.
Figure 7 shows the IFF failure loci in plane stress and its assumed evolution during fatigue cycling due to the reduction in material strength.

3.2.2 Transverse and shear modulus degradation of UD lamina

The response of the lamina to these stresses can be divided into three regimes. Figure 8 shows the typical IFF failure for each of these modes. For a typical application of GFRP the stresses in the through-the-thickness (Z) direction are very small. In this case the fracture plane in modes A and B is at 0° as shown in Figure 8.
In mode A the lamina pulls apart when IFF occurs due to the tensile normal load. Both the transverse normal modulus and the shear modulus of the lamina decrease sharply due to these cracks which are full ply thickness and rapidly multiply after initiation. The secant moduli have after IFF have been modelled previously for quasi-static applications as functions of strain exertion [21]. These equations are modified for use in predicting fatigue modulus as follows:

$$E_{\perp f} = \left(\frac{1 - \eta_{rE}}{1 + c_E \left(f_{E(IFF)} - 1 \right)^{\xi_E}} + \eta_{rE} \right) E_{\perp f(IFF)} \tag{11}$$

$$G_{\perp \| f} = \left(\frac{1 - \eta_{rG}}{1 + c_G \left(f_{E(IFF)} - 1 \right)^{\xi_G}} + \eta_{rG} \right) G_{\perp \| f(IFF)} \tag{12}$$

where $E_{\perp f}$ is the degraded transverse fatigue modulus, $G_{\perp \| f}$ is the degraded shear fatigue modulus, $f_{E(IFF)}$ (strain exertion) is the ratio of current strain level to strain level at IFF initiation (always greater than 1), $E_{\perp f(IFF)}$ and $G_{\perp \| f(IFF)}$ are the moduli at IFF initiation, η_{rE} and η_{rG} are the final fractions of the moduli remaining at infinite exertion and c_E, c_G, ξ_E, ξ_G are parameters which control the shape of the degradation curve.
In mode A (cf. Figs. 7 and 8) before IFF there is little or no degradation of transverse modulus; however there is significant degradation in shear modulus. There are also interaction effects of transverse stresses on shear modulus degradation. The shear fatigue modulus before IFF is again described based on an equation originally used to model secant modulus degradation [22] and modified as follows:

$$G_{\perp \| f} = \left(\frac{\left[f_E^{(\tau_{21})} + C^{(\sigma_2)} \left(f_E - f_E^{(\tau_{21})} \right) \right] - f_{E\tau hr}^{\tau_{21}}}{1 - f_{E\tau hr}^{\tau_{21}}} \right)^{n^{(\tau_{21})}} \times \left(G_{\perp \|} - G_{\perp \| f} \big|_{f_E^{(\tau_{21})} = 1} \right) \tag{13}$$

where $G_{\perp\parallel f}$ is the fatigue degraded shear secant modulus, $G_{\perp\parallel}$ is the original modulus during the linear part of the response, $G_{\perp\parallel f}|_{f_E^{(\tau_{21})}=1}$ is the shear fatigue modulus at IFF initiation with only shear loading applied, $f_E^{(\tau_{21})}$ is the stress exposure if only the current shear stress were applied, f_E is the stress exposure including both normal and shear stresses, $f_{Ethr}^{\tau_{21}}$ is a stress exposure threshold below which no damage occurs and $n^{(\tau_{21})}$ and $C^{(\sigma_2)}$ are factors which control the shape of the response. Equation (13) also describes the degradation of shear fatigue modulus in modes B and C before IFF.

Fatigue degradation of transverse modulus in compression (modes B and C of Figs. 7 and 8) before IFF is given by:

$$E_{\perp f} = \left(\frac{\left[f_E^{(\sigma_2)} + C^{(\tau_{21})} \left(f_E - f_E^{(\sigma_2)} \right) \right] - f_{Ethr}^{\sigma_2}}{1 - f_{Ethr}^{\sigma_2}} \right)^{n^{(\sigma_2)}} \times \left(E_\perp - E_{\perp f}|_{f_E^{(\sigma_2)}=1} \right) \quad (14)$$

where $E_{\perp f}$ is the degraded transverse fatigue modulus, $E_\perp$ is the original modulus during the linear part of the response, $E_{\perp f}|_{f_E^{(\sigma_2)}=1}$ is the transverse fatigue modulus at IFF initiation with only normal loading applied, $f_E^{(\sigma_2)}$ is the stress exposure if only the current normal stress were applied, f_E is the stress exposure including both normal and shear stresses, $f_{Ethr}^{\sigma_2}$ is a threshold below which no damage occurs and $n^{(\sigma_2)}$ and $C^{(\tau_{21})}$ are factors which control the shape of the response. After IFF in mode B the faces of the cracks do not separate as they are pressed together by the compressive (normal) stress. Therefore the transverse modulus will not see the sharp decrease typical of mode A. In this work it is assumed here that the transverse modulus degradation continues to follow Equation 14 after IFF in mode B. The shear modulus is expected to degrade sharply after IFF in mode B and follow Equation 12.

It has been shown [3] that when out of plane normal stress (σ_3) is small the fracture planes in modes A and B are always perpendicular to the lamina (θ_{fp} = 0°). In mode C however the high compressive stresses will cause cracks on a fracture plane up to 51°. This can cause a wedge effect leading to delamination and local buckling and thereby precipitate failure of the laminate. In this paper, if IFF is predicted in mode C total laminate failure is assumed to occur and the analysis is stopped. Before IFF in mode C the transverse and shear moduli are assumed to degrade in a manner consistent with equations 13 and 14.

3.2.3 FE modelling details

Figure 9 shows a unit cell model of a balanced, symmetric, quasi isotropic GFRP laminate ($[45/135/90/0]_s$) to mimic the experimental laminate. The model is a cube with 1.92 mm edge length and includes 8 plies with the material orientation in each ply specified in 45° increments. Each 0.240 mm thick ply has three 8-node brick elements through the thickness. Mesh convergence studies established this degree of mesh refinement to be sufficient for converged laminate stresses.

The material behaviour including fatigue damage is implemented here and calibrated via a user material subroutine (UMAT) in the commercial FE code Abaqus. Symmetric boundary conditions are used on 3 faces to reduce modelling effort resulting in a 1/8th model of the laminate. This unit cell is assumed to be embedded in a large QI laminate which experiences uniaxial tensile loading. Therefore it is assumed that all faces of the cube remain plane and this constraint is imposed on the 3 faces not constrained by symmetric boundary conditions. Initial damage to fibre direction modulus with a maximum level of 0.1% is randomly distributed in every element of the model. Following the recommendation by [21] in this model the major Poisson's ratio remains constant (ν_{12} = 0.24). The Poisson's ratio between the 3 and 2 directions is also kept constant ($\nu_{32} = 0.35$). All other ratios are recalculated at the beginning of each iteration based on the damage level of the relevant moduli.

3.2.4 Calibration of material constants for fatigue model

Table 1 shows the material strength values identified for the model. The fatigue evolution data used are based on experimental results reported in [16] and [23]. Table 2 shows the values used for the parameters in Equations 13 and 14. These are from refs. [22] and [24] except $E_{\perp f}|_{f_E^{(\sigma_{22})}=1}$ in the case where the transverse stress is positive which is given a small nominal degradation. Table 3 shows the values used for the parameters in Equations 11 and 12 based on data from [21]. Table 4 shows the values used in degrading the fibre direction modulus based on data presented in [25].

4 Results

Figure 10 shows the measured first and last stress-strain cycles of an R = 0.1 uniaxial fatigue test with a maximum stress of 155 MPa for a QI laminate of epoxy/E-glass tested here. Both secant and fatigue modulus decrease while irrecoverable strain increases during fatigue cycling.

Figure 11 shows the evolution of secant modulus for a fatigue test at 139 MPa (maximum stress) compared to predicted (from the unit cell laminate model) secant modulus behaviour. Clearly the predicted response captures the overall modulus degradation in the first cycle and follows the evolution of degradation with subsequent cycles until failure at less than 10^6 cycles. The degradation in the first cycle is primarily caused by matrix micro-cracking before IFF in the 45° and 90° plies and by IFF cracking itself in the 90° ply as it is being loaded for the first time. The 45° plies may also experience IFF depending on the loading level. Subsequent fatigue cycling continues the modulus degradation in the 45° and 90° plies. Fatigue cycling also causes damage to the 0° plies which undergo sustained modulus reduction until very near their end of life when they experience rapid degradation.

It is also possible to predict fatigue modulus with this model. This requires a new set of parameters for post-IFF degradation and dropping of the 1-direction creep strain from the model. It also requires an assumption that the percentage fatigue modulus degradation in transverse and shear before IFF is half that of secant modulus. The assumed modulus values at IFF and the new set of parameters for Equations 13 and 14 which have been developed here to predict fatigue modulus evolution after IFF are detailed in Table 5.

Figure 12 shows the predicted fatigue modulus compared to the experimental result for the same test as Figure 11. The drop in modulus on the first cycle is 2.7 GPa or 12% at this stress level. The standard method for measuring modulus of a coupon uses a straight line fit to the stress strain curve between 0.05% and 0.25% strain. As some damage takes place in this region the modulus measured by the standard method will be lower than the initial modulus. In the case of the fatigue test shown in Figure 11 it is almost 10% lower than the initial modulus.

If the standard modulus is used as the baseline then the drop in modulus in the first 5 cycles is found to be 3% and the drop in modulus before failure is 36%. Within the laminate model three mechanisms contribute to the drop in modulus during fatigue cycling. First, the transverse and shear strength of the material are reduced. This promotes increased cracking even though the stresses are constant or reducing. Second, the fibre direction modulus reduces which has a direct impact on the stiffness of the laminate. Thirdly, the increases in strain caused by these two previous damage mechanisms, in turn cause increased damage and loss of stiffness.

Figure 13 shows the comparison of predicted and measured modulus evolution at a maximum stress of 219 MPa. In this case the modulus of the coupon is reduced by 12% from the standard modulus in the first few cycles and by 34% before failure. The model accurately predicts the drop in modulus on the first cycle but overpredicts the drop in modulus before failure by an additional 16%.

Figure 14 shows modulus degradation due to fatigue damage from tests on a QI vinylester/E-glass laminate. A 52.5 mm gauge length extensometer, which was attached to the coupon at various intervals during the fatigue test was used to measure the evolution of modulus. The evolution of irrecoverable strain was evaluated from the measured change in length of the coupon.

In composite laminates during fatigue cycling, the damage tends to be distributed over the entire gauge length of the coupon for a significant fraction of the fatigue life. Figures 15a and 15b show the re-predicted evolution of fatigue damage in a 0° ply for the R = 0.1 test with maximum stress of 139 MPa. These figures show that the areas with predicted damage at an early fraction of the coupon life do not remain the only damage zones steadily growing until fracture. Instead they have a slower rate of damage accumulation and other areas with less damage initially then catch up. This effect is not seen in fatigue testing of individual unidirectional plies, where damage tends to remain localised (often at the stress concentration produced by the grips) until failure. The pattern of damage distribution continues in the laminate until some significant damage accumulates in one area weakening that area below a critical level. Subsequently the damage further localises in this area leading rapidly to failure of the coupon. This effect can be seen in the sharp decrease in modulus at the end of the fatigue life in Figures 11 and 12.

Figure 16 shows the predicted evolution of transverse and shear stiffness damage of an element in a 45° ply. This clearly shows the damage in the first cycle and then further cumulative damage during fatigue cycling, leading to low transverse and shear stiffness's in this ply toward the end of the fatigue life.

Figure 17 shows the successful validation of fatigue life predictions given by the finite element analysis for QI glass/epoxy coupons under uniaxial tensile (R = 0.1) loading,

compared with the results from the fatigue test experiments and the median curve fit to those data. Clearly, the fatigue damage model gives excellent predictions for coupon life. At 219 MPa the secant version of the model predicts a life of 4,240 cycles; by comparison, for the same life, the median curve fit to the experimental results corresponds to a 2% lower stress. At high cycles, a stress of 139 MPa gives a predicted life of 345,447 cycles whereas the experimental curve fit would predict this life to occur with a 3% higher stress. In terms of fatigue life for a given stress, life predictions are within a factor of 2 of those given by the curve fit to the experimental results. The model life predictions based on fatigue modulus degradation are slightly less accurate but still within the factor of two.

5 Conclusion

A new model for fatigue damage evolution in fibre reinforced polymer composites is presented. An existing quasi-static method for prediction of (i) inter fibre fracture and (ii) its effects on transverse and shear stiffness for quasi static cases has been adapted to model the significant damage induced during the loading phase of the first fatigue cycle on GFRP laminates. This method is further extended to predict the continued damage to those same matrix-dominated moduli during fatigue cycling. Most of the damage to the matrix dominated moduli takes place in the off axis plies and the key effect is the extent to which load is transferred onto the on-axis plies. The SN curve for on-axis fatigue of GFRP has quite a small slope and therefore even small increases in the stress experienced by the on-axis plies of a laminate has a large effect on fatigue life. Fibre direction damage to both strength and modulus are incorporated into the model and creep strain induced by tensile loading is also modelled. All these predictions are made at the ply level thereby allowing a laminate of any configuration to be modelled and its behaviour under fatigue cycling to be predicted. An example of a QI epoxy / E-glass laminate is considered and the results compared to parallel experimental testing. The following conclusions are reached

- Stiffness degradation in the first few fatigue cycles of QI laminates varies between 0% and 10% below the value measured by the standard modulus test; the larger value is associated with the higher maximum fatigue stresses. The model described herein is able to predict this drop in modulus accurately over a range of fatigue stress levels.
- Overall reductions in laminate stiffness of 25 to 35% before final fracture are measured with widely distributed damage seen to be the mechanism that facilitates this. The model makes good predictions for this phenomenon at lower stress levels although it over-predicts the degradation by 50% at high stress levels.
- The model is seen to accurately predict fatigue life relative to the experimentally measured fatigue life.

6 References

[1] R. Talreja, 'Fatigue of Composite Materials: Damage Mechanisms and Fatigue-Life Diagrams', *Proceedings of the Royal Society of London. A. Mathematical and Physical Sciences*, vol. 378, no. 1775, pp. 461 –475, Nov. 1981.

[2] J. Tong, F. J. Guild, S. L. Ogin, and P. A. Smith, 'On matrix crack growth in quasi-isotropic laminates--I. Experimental investigation', *Composites Science and Technology*, vol. 57, no. 11, pp. 1527–1535, 1997.

[3] A. Puck and H. Schürmann, 'Failure analysis of FRP laminates by means of physically based phenomenological models', *Composites Science and Technology*, vol. 62, no. 12–13, pp. 1633–1662, Sep. 2002.

[4] J. Tong, F. Guild, S. Ogin, and P. Smith, 'Off-axis fatigue crack growth and the associated energy release rate in composite laminates', *Applied Composite Materials*, vol. 4, no. 6, pp. 349–359, 1997.

[5] S. Adden and P. Horst, 'Damage propagation in non-crimp fabrics under bi-axial static and fatigue loading', *Composites Science and Technology*, vol. 66, no. 5, pp. 626–633, May 2006.

[6] D. Hull and T. W. Clyne, *An Introduction to Composite Materials*, 2nd ed. Cambridge University Press, 1996.

[7] M. . Hinton, A. . Kaddour, and P. . Soden, 'A comparison of the predictive capabilities of current failure theories for composite laminates, judged against experimental evidence', *Composites Science and Technology*, vol. 62, no. 12–13, pp. 1725–1797, Sep. 2002.

[8] R. Martin, 'Delamination fatigue', in *Fatigue in composites: science and technology of the fatigue response of fibre-reinforced plastics*, Woodhead Publishing, 2003.

[9] B. D. Agarwal and L. J. Broutman, *Analysis and Performance of Fiber Composites, 2nd Edition*, 2nd ed. Wiley-Interscience, 1990.

[10] A. E. Antoniou, C. Kensche, and T. P. Philippidis, 'Mechanical behaviour of glass/epoxy tubes under combined static loading. Part I: Experimental', *Composites Science and Technology*, vol. 69, no. 13, pp. 2241–2247, Oct. 2009.

[11] R. Talreja, 'Damage and fatigue in composites - A personal account', *Composites Science and Technology*, vol. 68, no. 13, pp. 2585–2591, Oct. 2008.

[12] J. Degrieck and W. Van Paepegem, 'Fatigue damage modeling of fibre-reinforced composite materials: Review', *Applied Mechanics Reviews*, vol. 54, no. 4, p. 279, 2001.

[13] C. Schuecker and H. E. Pettermann, 'A continuum damage model for fiber reinforced laminates based on ply failure mechanisms', *Composite Structures*, vol. 76, no. 1–2, pp. 162–173, Oct. 2006.

[14] X. S. Sun, A. Haris, V. B. C. Tan, T. E. Tay, S. Narasimalu, and C. N. Della, 'A multi-axial fatigue model for fiber-reinforced composite laminates based on Puck's criterion', *Journal of Composite Materials*, vol. 46, no. 4, pp. 449–469, Feb. 2012.

[15] V. A. Passipoularidis, T. P. Philippidis, and P. Brondsted, 'Fatigue life prediction in composites using progressive damage modelling under block and spectrum loading', *International Journal of Fatigue*, vol. 33, no. 2, pp. 132–144, Feb. 2011.

[16] J. Wedel-Heinen et al., 'Optimat report OB_TG6_R002 rev. 8', 2006.

[17] T. P. Philippidis and V. A. Passipoularidis, 'Residual strength after fatigue in composites: Theory vs. experiment', *International Journal of Fatigue*, vol. 29, no. 12, pp. 2104–2116, Dec. 2007.

[18] Broutman, L.J and Sahu, S., 'A New Theory to Predict Cumulative Fatigue Damage in Fiberglass Reinforced Plastics', in *Composite Materials: Testing and Design (second conference)*, ASTM International, 1972.

[19] H. Mao and S. Mahadevan, 'Fatigue damage modelling of composite materials', *Composite Structures*, vol. 58, no. 4, pp. 405–410, Dec. 2002.
[20] A. Puck, J. Kopp, and M. Knops, 'Guidelines for the determination of the parameters in Puck's action plane strength criterion', *Composites Science and Technology*, vol. 62, no. 3, pp. 371–378, Feb. 2002.
[21] M. Knops and C. Bögle, 'Gradual failure in fibre/polymer laminates', *Composites Science and Technology*, vol. 66, no. 5, pp. 616–625, May 2006.
[22] A. Puck and M. Mannigel, 'Physically based non-linear stress–strain relations for the inter-fibre fracture analysis of FRP laminates', *Composites Science and Technology*, vol. 67, no. 9, pp. 1955–1964, Jul. 2007.
[23] C. W. Kensche, 'Fatigue of composites for wind turbines', *International Journal of Fatigue*, vol. 28, no. 10, pp. 1363–1374, Oct. 2006.
[24] P. Soden, 'Lamina properties, lay-up configurations and loading conditions for a range of fibre-reinforced composite laminates', *Composites Science and Technology*, vol. 58, no. 7, pp. 1011–1022, Jul. 1998.
[25] T. P. Philippidis, E. N. Eliopolus, A. A. Antoniou, and V. A. Passipoularidis, 'Material model incorporating loss of strength and stiffness due to fatigue: preliminary results from fe model implementation', *Upwind report deliverable 3.3.1*, Jul. 2003.

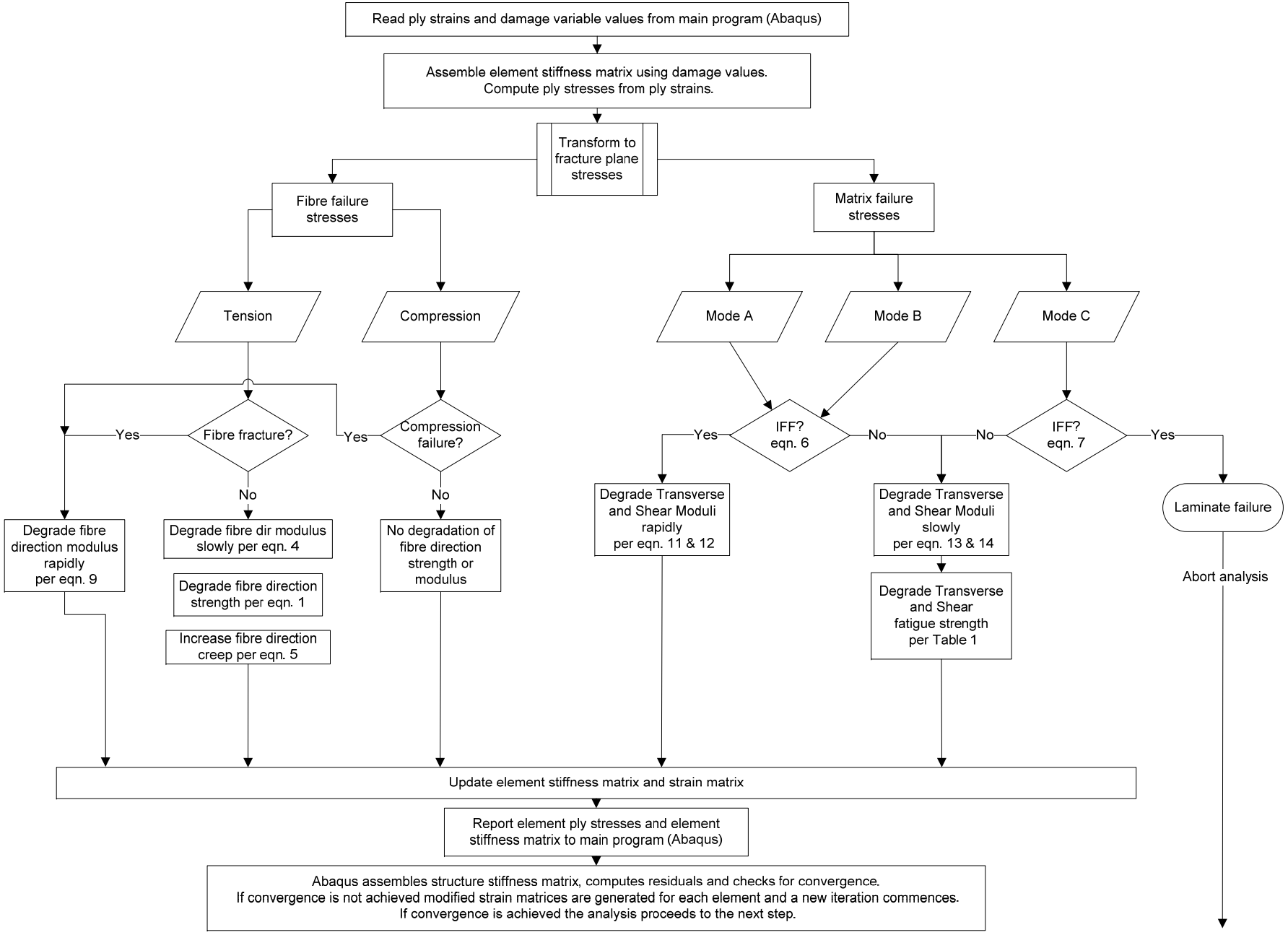

Figure 1. Flowchart of FE subroutine method

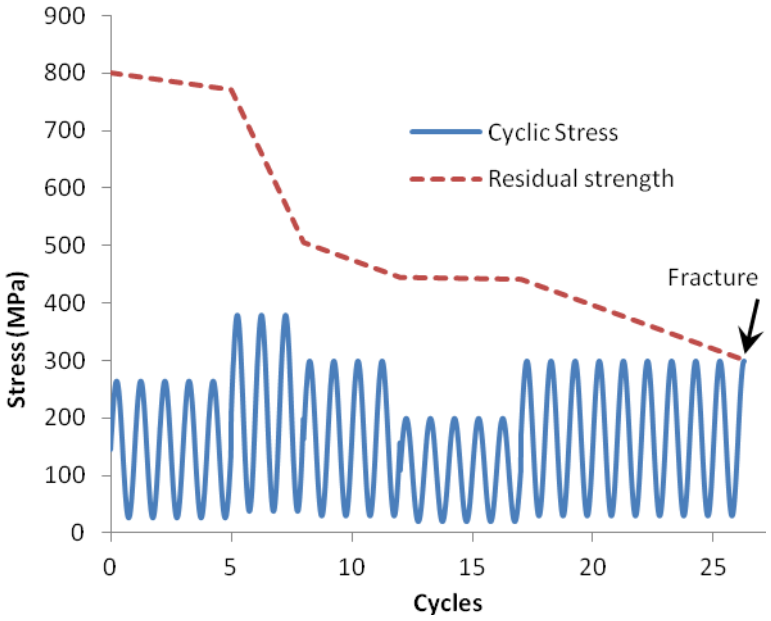

Figure 2. Schematic of strength degradation in 0° plies during fatigue

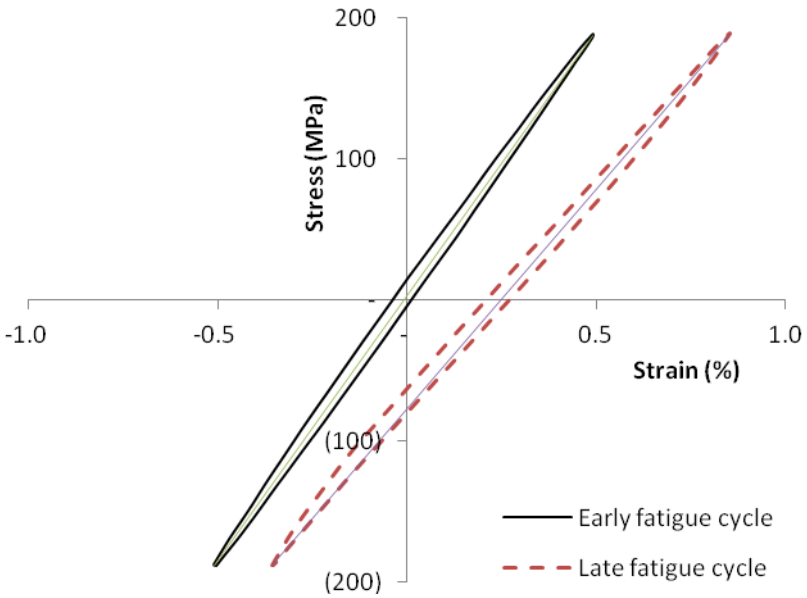

Figure 3. Early and late stress strain cycles during fatigue life of UD GFRP, *after* [25]

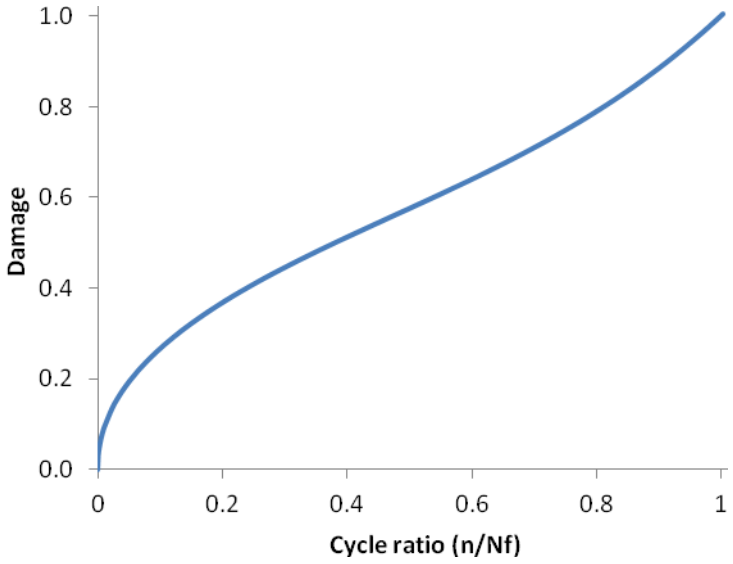

Figure 4. S-shaped damage curve

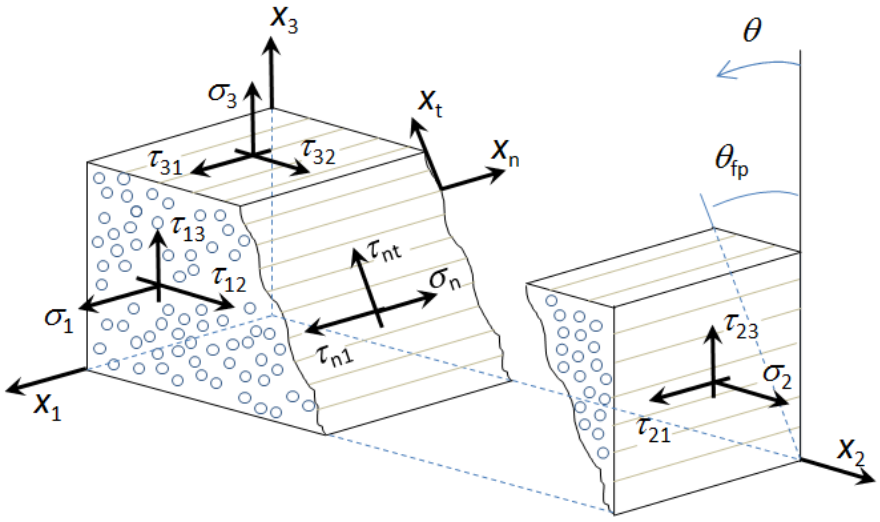

Figure 5. Fracture plane coordinate system, *after* Puck et al. [17].

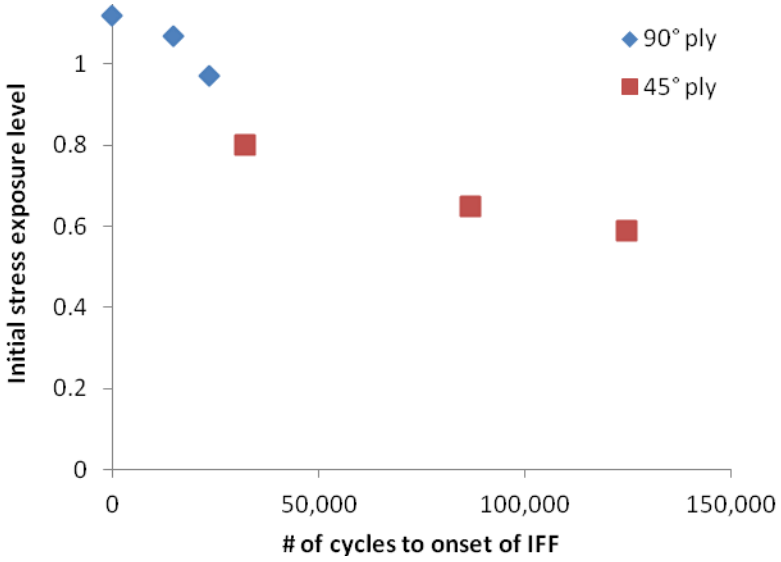

Figure 6. Initial stress exposure level versus IFF onset in fatigue of QI plies

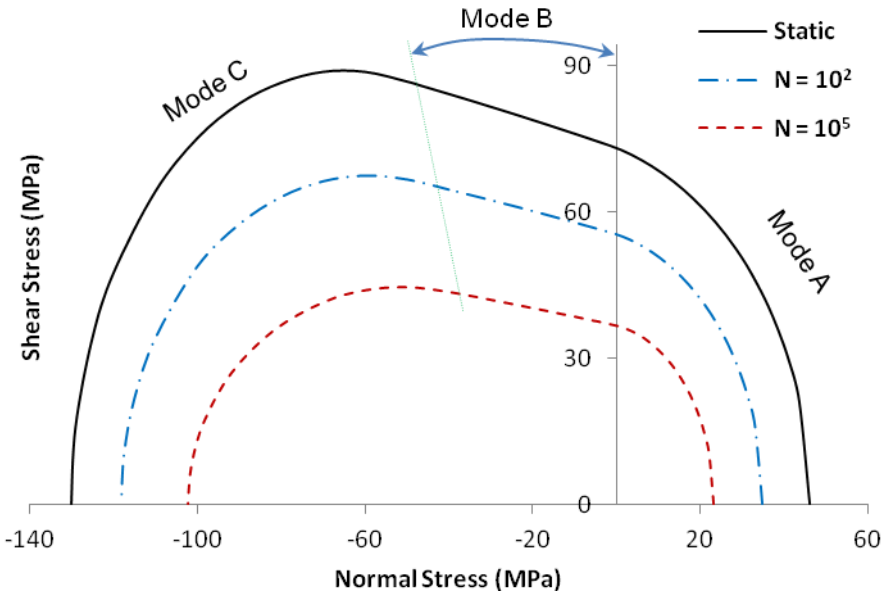

Figure 7. Evolution of IFF loci of UD GFRP lamina under fatigue cycling

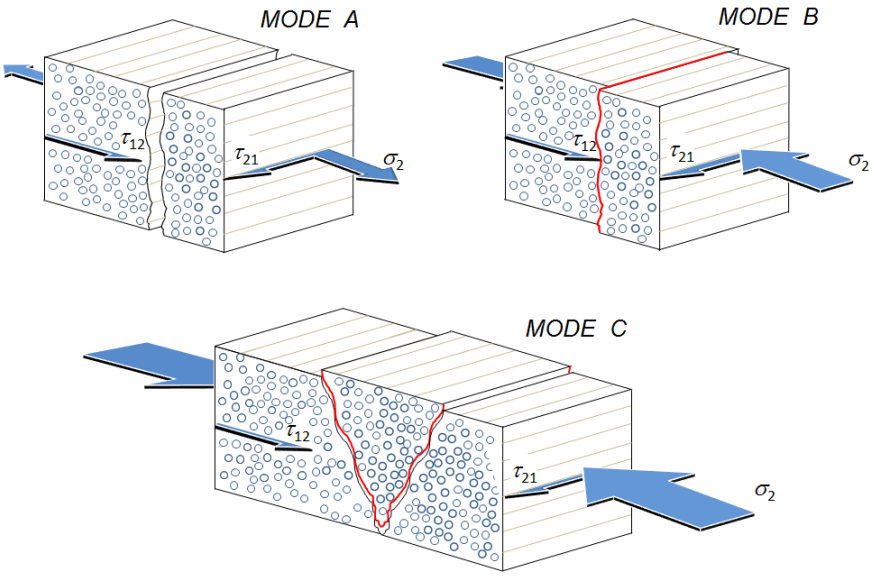

Figure 8. Typical IFF failure modes of UD FRP lamina (after [20])

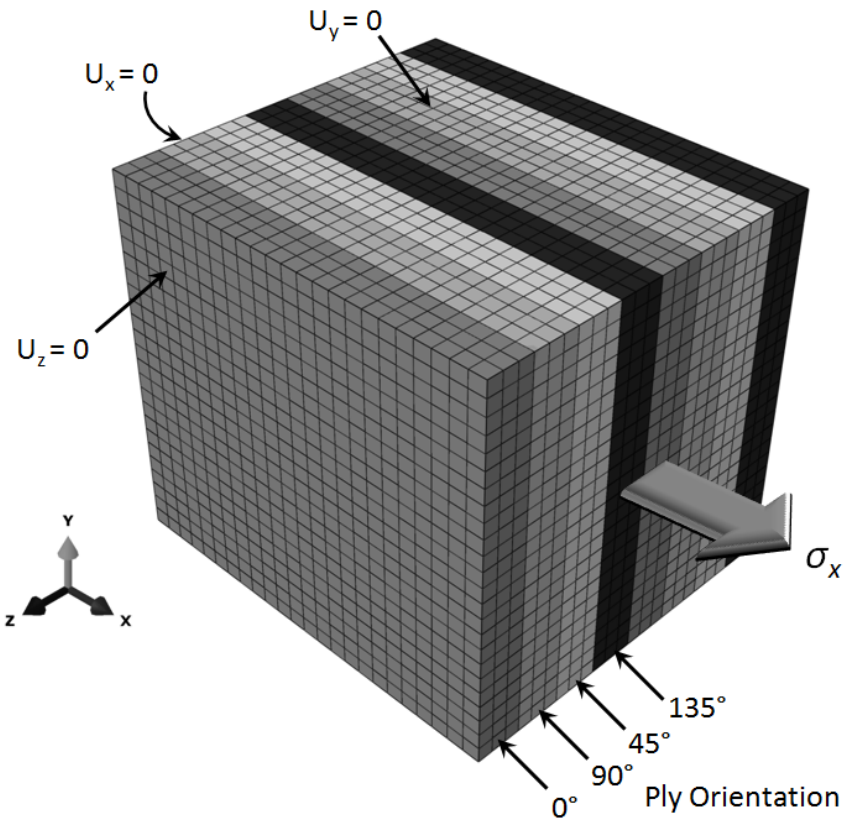

Figure 9. Unit cell model of QI epoxy/E-glass

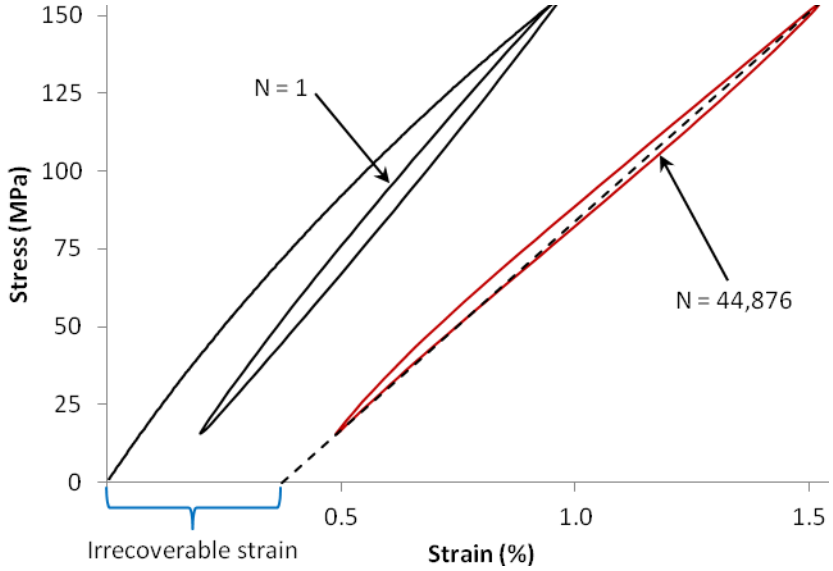

Figure 10. Measured stress-strain loops of $R = 0.1$ fatigue test of epoxy/E-glass.

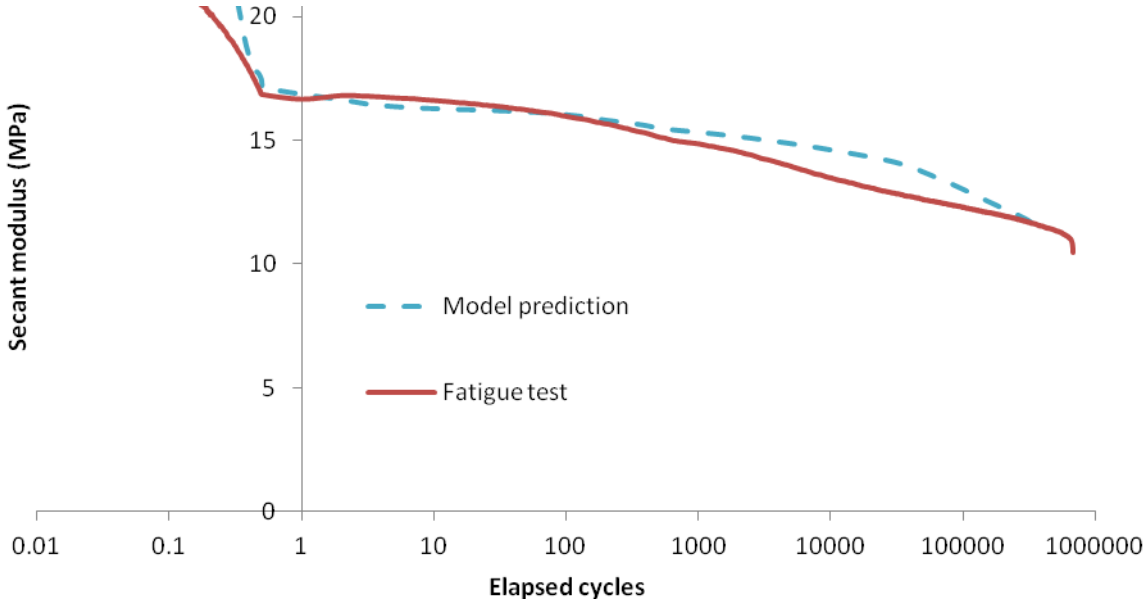

Figure 11. Predicted and measured secant modulus during $R = 0.1$ fatigue testing of a QI epoxy/E-glass laminate at 139 MPa maximum stress

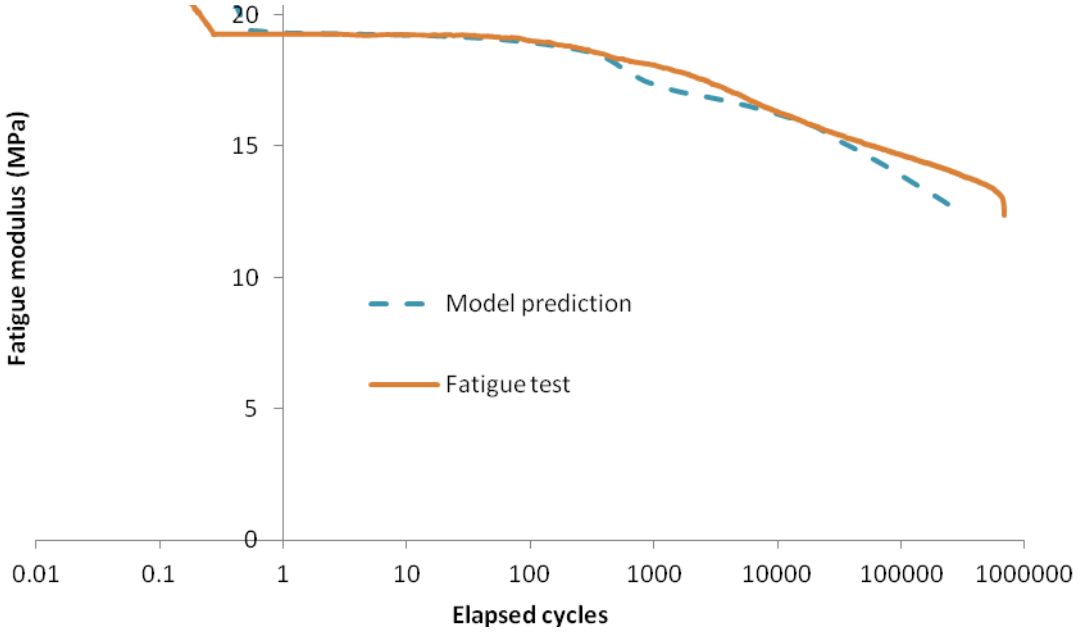

Figure 12. Validation of predicted fatigue modulus against measured fatigue modulus from fatigue testing of a QI epoxy/E-glass laminate at 139 MPa maximum stress

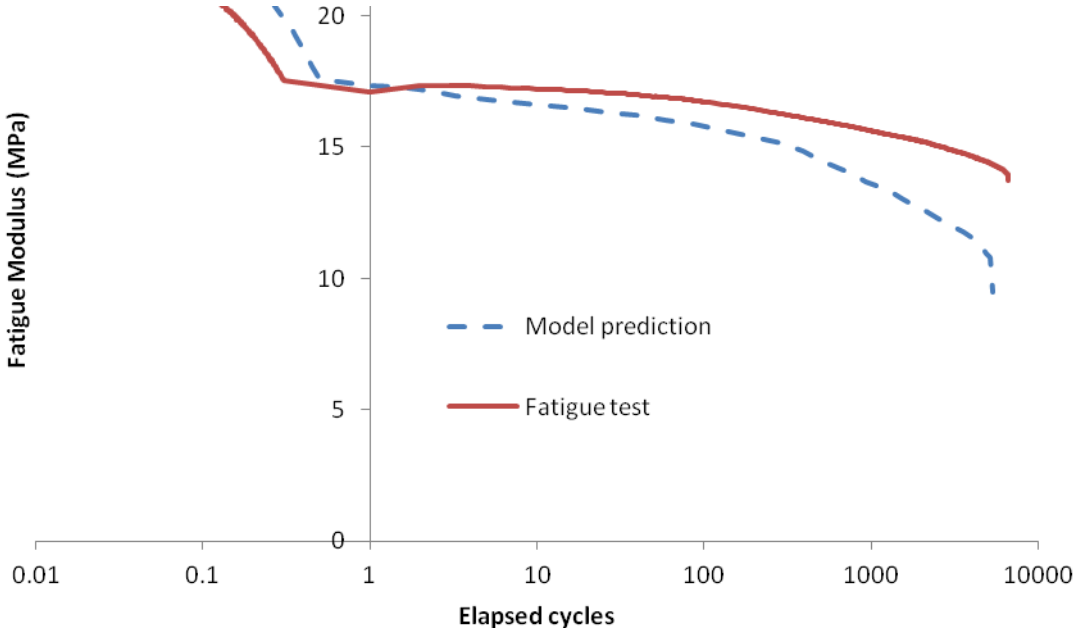

Figure 13. Validation of predicted fatigue modulus against measured fatigue modulus from fatigue testing of a QI epoxy/E-glass laminate at 219 MPa maximum stress

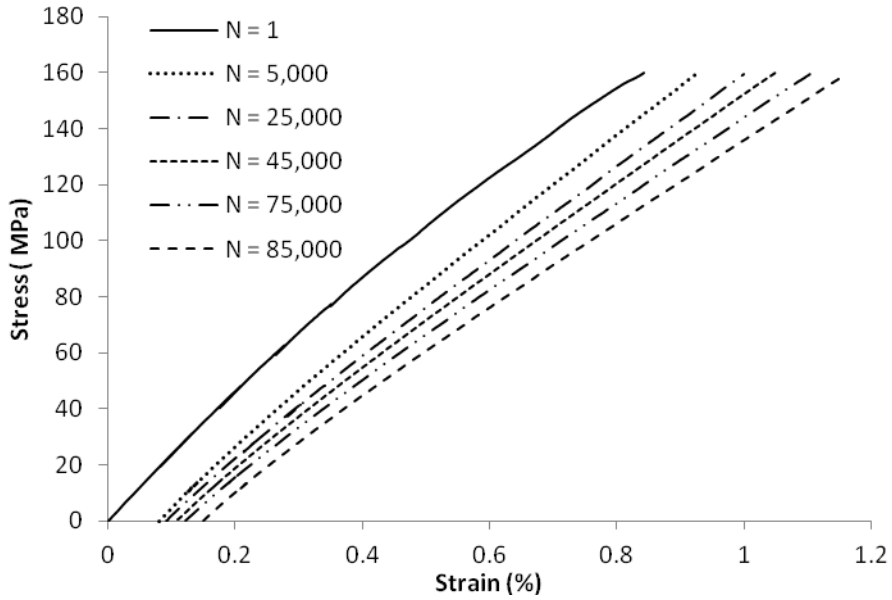

Figure 14. Extensometer determined stress-strain curves at intervals during fatigue testing

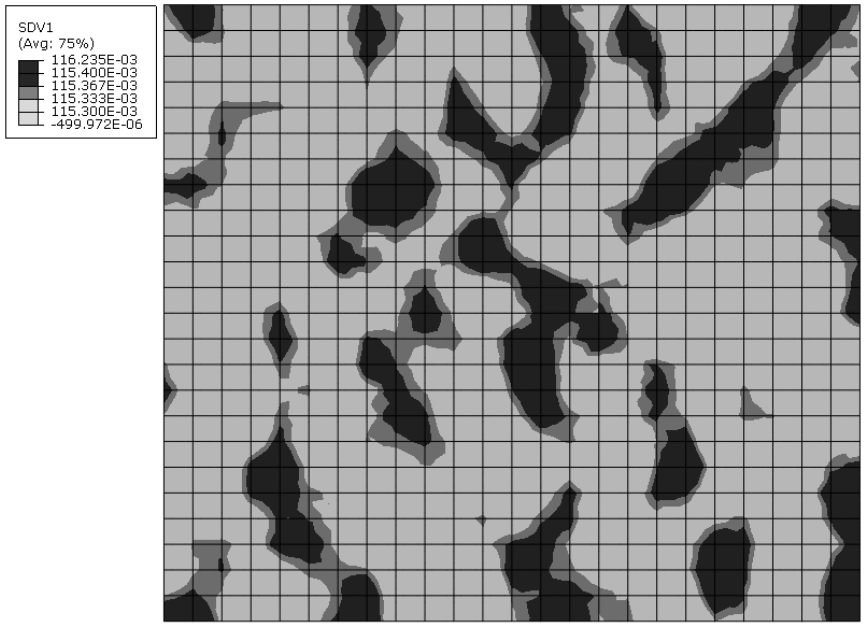

(a)

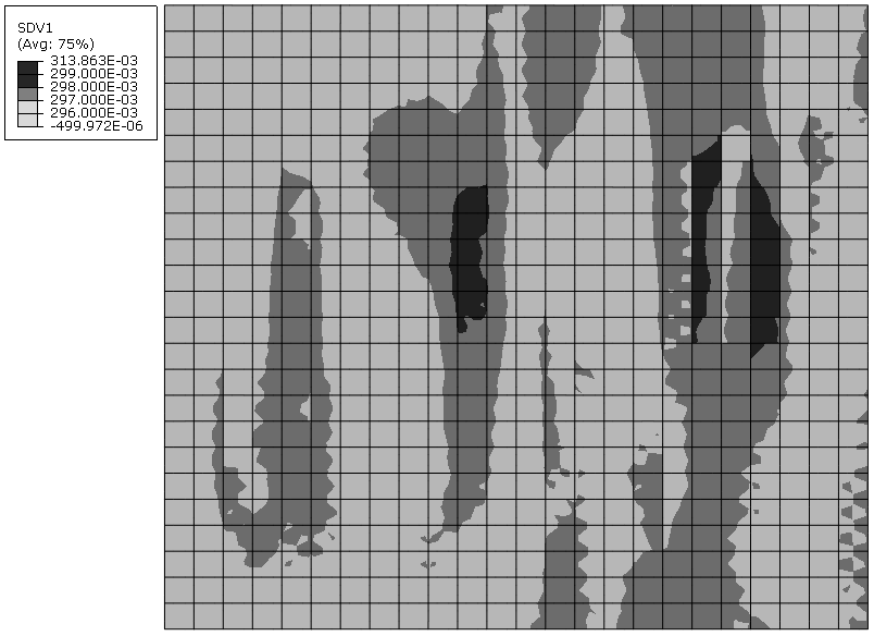

(b)

Figure 15 Two dimensional images of predicted damage in a 0° ply from 3D unit cell model of Fig. 9 at (a) 12,099 cycles and (b) 254,184 cycles

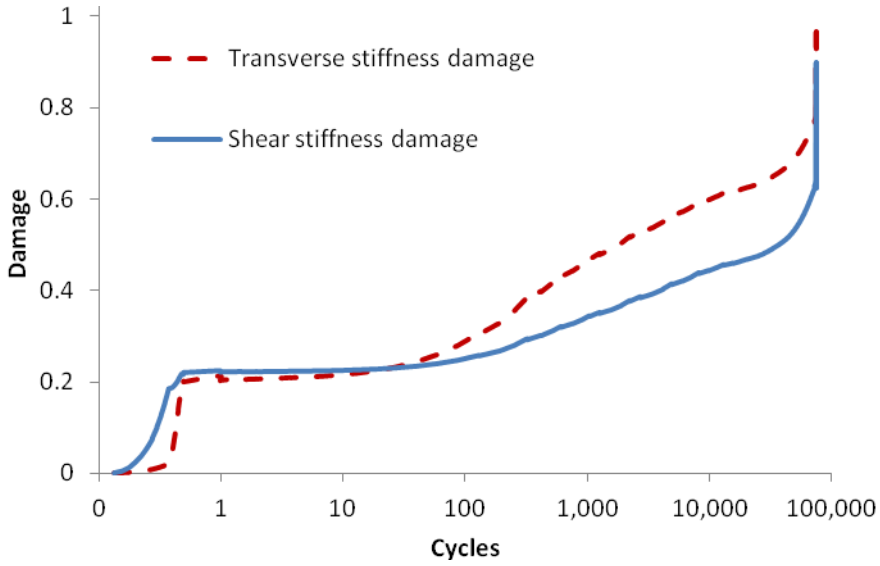

Figure 16. Predicted transverse and shear stiffness damage in 45° ply element.

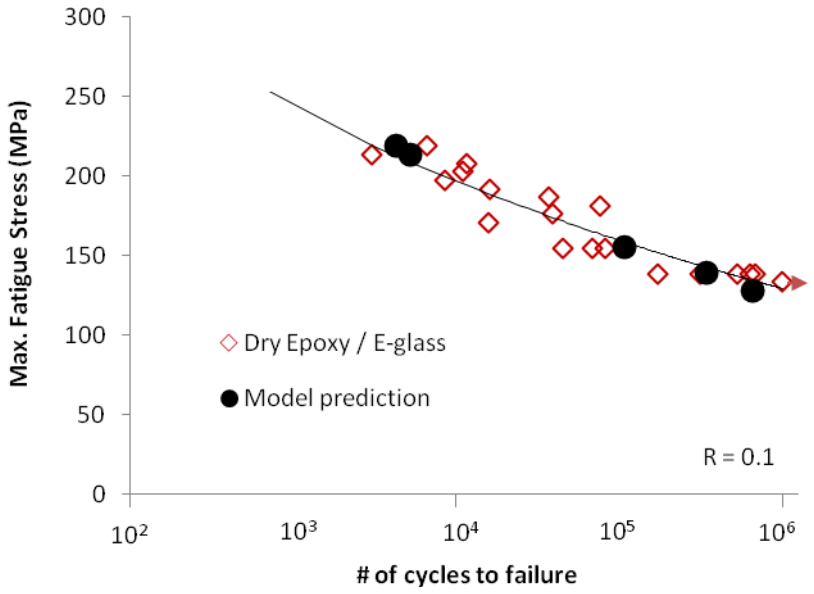

Figure 17. Validation of finite element predictions for life against experimental results.

Table 1 Identified strength data for UD epoxy/E-glass lamina with V_f =50%

Parameter	Static Failure Value	Fatigue	
		A	B
$R_{\parallel}^{(+)}$	778 MPa [16]	1120 MPa	0.1003
$R_{\perp}^{(+)}$	46 MPa [21]	73 MPa	0.1003
$R_{\perp}^{(-)}$	145 MPa [20]	185 MPa	0.0407
$R_{\perp\parallel}$	72 MPa [22]	114 MPa	0.1003
$R_{\perp\perp}^{f}$	Eqn. 8	Eqn. 8	
$p_{\perp\parallel}^{(-)}$	0.3 [20]	0.3 [20]	
$p_{\perp\parallel}^{(+)}, p_{\perp\perp}^{(+)}, p_{\perp\perp}^{(-)}$	0.25 [20]	0.25 [20]	

Table 2. Pre-IFF secant modulus degradation parameters

$E_{\perp}$	$E_{\perp s}\|_{f_E^{(\sigma_2)}=1}$ tension	$E_{\perp s}\|_{f_E^{(\sigma_2)}=1}$ compression	$G_{\perp\parallel}$	$G_{\perp\parallel s}\|_{f_E^{(\tau_{21})}=1}$	$f_{Ethr}^{\sigma_2}, f_{Ethr}^{\tau_{21}}$	$C^{(\tau_{21})}, C^{(\sigma_2)}$	$n^{(\tau_{21})}$	$n^{(\sigma_2)}$
13.25 GPa	12.6 GPa	10 Gpa [22]	4.6 GPa	1.52 GPa [24]	0.3 [22]	0.6 [22]	2.0 [22]	3.0 [22]

Table 3. Post-IFF modulus degradation parameters

η_{rE}	η_{rG}	ξ_E	ξ_G	c_E	c_G
0.03 [21]	0.25 [21]	1.3 [21]	1.5 [21]	5.3 [21]	0.70 [21]

Table 4. Fibre direction damage parameters identified from data presented in [25]

$\Delta\varepsilon$	q	m1	m2	$\varepsilon_{\perp f}$
$0.074\sigma_{1,max} + 8.74$	0.8	0.2	8.7	0.2%

Table 5. Fatigue modulus degradation parameters

$E_{\perp f}\|_{f_E^{(\sigma_2)}=1}$ tension	$E_{\perp f}\|_{f_E^{(\sigma_2)}=1}$ compression	$G_{\perp\parallel f}\|_{f_E^{(\tau_{21})}=1}$	η_{rE}	η_{rG}	ξ_E	ξ_G	c_E	c_G
12.9 GPa	11.7 Gpa	3.0 GPa	0.001	0.125	1.17	1.5	0.88	0.30